Algae adhesion onto silicone is sensitive to environment-induced surface restructuring

Zhijing Wan, Md. Shafiul Azam, Shea Wyatt, Kaitlyn Ramsay, Jaime L. Korner, Katherine S. Elvira, Rajkumar Padmawar, Diana Varela & Dennis K. Hore

2021

Algae Adhesion onto Silicone is Sensitive to Environment-Induced Surface Restructuring

Zhijing Wan,[†] Md. Shafiul Azam,[†] Shea Wyatt,[‡] Kaitlyn Ramsay,[†] Jaime L. Korner,[†] Katherine S. Elvira,[†] Rajkumar Padmawar,[¶] Diana Varela,[‡,§] and Dennis K. Hore[*,†,‖]

[†]*Department of Chemistry, University of Victoria, Victoria, British Columbia, V8W 3V6, Canada*

[‡]*Department of Biology, University of Victoria, Victoria, British Columbia, V8W 2Y2, Canada*

[¶]*ASAsoft (Canada) Inc., 179-2945 Jacklin Road Suite 221, Victoria, British Columbia, V9B 6J9, Canada*

[§]*School of Earth and Ocean Sciences, University of Victoria, Victoria, British Columbia, V8W 2Y2, Canada*

[‖]*Department of Computer Science, University of Victoria, Victoria, British Columbia, V8W 3P6, Canada*

E-mail: dkhore@uvic.ca

Abstract

Resistance to algae contamination is an important characteristic of insulators used in overhead power distribution in coastal environments. It is therefore important to understand the parameters governing algae adhesion onto polymer insulator materials such as silicone. Flow-cell based shear experiments were conducted in order to characterize the adhesion strength of algae onto polydimethylsiloxane surfaces, comparing fresh polymer substrates with those that have been soaked in water and saline solutions for one month. Both freshwater algae and a seawater species could withstand considerably less drag force and were therefore more easily removed when the polymer was soaked in salt water. The polymer surface was found to be unaltered in terms of its roughness, contact angle, and lack of water uptake; no macroscopic surface characterization was therefore able to account for the differences in cell adhesion strength resulting from the soaking treatment. Surface-specific nonlinear vibrational spectroscopy, however, revealed subtle differences in the orientation of surface methyl groups that resulted from the water and saline exposure.

Introduction

Polymer insulators, also known as composite insulators, are attractive alternatives to traditional glass or ceramic devices for overhead power distribution, a critical component of the global electrical grid.[1,2] Hydrophilic materials suffer from water ingress that ultimately leads to cracking and premature device failure. Polymers such as silicones offer enhanced and prolonged hydrophobicity and therefore lower operating costs, in addition to a greener manufacturing footprint.[3] Silicone insulators are also suitable for a wide variety of climates, including those with extreme temperature variation, and those subject to deicing salts in winter conditions.[4,5] However, one area that remains particularly challenging is mitigation of algae adhesion when the devices are installed in coastal areas, as the fouling of bioorganisms rapidly degrades the material surfaces.[6–11] Although some field reports exist, there is a lack of data on algae-silicone interactions, particularly under environmental conditions such as exposure to water and high voltage. Silicone polymers are also widely used in microfluidic devices, including in applications where cells are adhered in a variety of aqueous environments.[12,13]

This is a fundamental materials science problem as understanding the surface properties of polymers is related to, but not completely predicted from, the bulk properties of the material. Many powerful techniques are available for characterizing polymer surfaces, but those that offer molecular information are especially valuable when they are able to probe the surface in an environment that is analogous to the application conditions. In this case, the initial adhesion of cells occurs at polymer-aqueous interfaces. It has been well-established that the molecular structure of polymers may be substantially altered according to the adjacent solution conditions.[14–17] For such studies, the nonlinear vibrational technique of visible-infrared sum frequency generation (SFG) offers molecular fingerprints of buried polymer-aqueous interfaces, and the ability to characterize the orientation of specific surface functional groups. SFG spectroscopy has therefore been valuable in characterizing the surface of polydimethylsiloxane (PDMS) films in their native state, and under different treatment conditions.[18–24]

We have recently developed an imaging platform that consists of a flow cell with variable wall

shear coupled with microscope-based data collection and software for cell tracking that enables the adhesion strength of algae to be measured by quantifying drag force experienced by adhered cells.[25] We now use this setup to study the adhesion of two algae on PDMS surfaces. *Botryococcus Braunii* is a freshwater green alga, and strongly adheres to surfaces that are exposed to spray from lakes and rivers. *Thalassiosira rotula* is a diatom found in marine environments around the globe.[26,27] Although less sticky than the benthic diatom species that are commonly found in algae biofilms, *T. rotula* is present throughout the water column and is likely to be a component of algae assemblages that can affect substrates exposed to seawater spray. For each of these algae, we have assembled the flow cells using PDMS substrates prepared under three conditions: using freshly-prepared films, and with those exposed to water and salt water for one month. In order to understand the differences in adhesion behaviour, we have characterized the PDMS surfaces before and after aqueous exposure using a variety of methods, including SFG spectroscopy.

Methods

Algae cultures and sample preparation

B. braunii (UTEX 572) was obtained from the Culture Collection of Algae at the University of Texas at Austin. The cells were cultivated as batch cultures in BG-11 nutrient medium[28] at 20 °C under a 12:12 ratio light:dark cycle using an irradiance level of 15.6 ± 2.22 μmol photons$\cdot$m$^{-2}\cdot$s^{-1}. The pH of the medium was adjusted to 7.6 ± 0.1 using 1 M NaOH and 0.1 M HCl. Subculture was done every 4 to 5 weeks by inoculating 2 mL of cell culture to 250 mL new medium. To prepare cultures for adhesion experiment, cells in their log phase, around 6–8 d were collected for morphology evaluation and adhesion strength experiments. 1 mL of cell culture was collected in log phase and was sonicated for 30 s using 1 s pulses with a 1 s delay between pulses. The culture was centrifuged at 3000 rpm for 5 min, washed twice and re-suspended in phosphate buffered saline containing 1.62 mM KH_2PO_4, 6.49 mM K_2HPO_4, and 1.35 mM NaCl. The PBS was prepared to match the pH of BG-11. Finally, the culture was re-suspended in 1 mL BG-11

medium in preparation for adhesion characterization. The pelagic diatom *T. rotula* (CCMP3362) was obtained from the National Center for Marine Algae and Microbiota (Bigelow Laboratory, ME). The culture was maintained in exponential growth through semi-continuous batch culturing at 14 °C, under 65 μmol photons$\cdot$m$^{-2}\cdot$s^{-1} with a 13:11 light to dark cycle in an enriched seawater medium.[29] Anhydrous and hydrated salts were dissolved separately in deionized (DI) water and then combined before the addition of macronutrient, trace metal, and vitamin solutions. The medium was bubbled with filtered air to adjust the pH to ≈ 8.2 and then sterilized with a 0.2 μm VacuCap (Pall Corporation, NY) filtration device. Diatoms were subsampled near the end of the exponential phase for use in the adhesion experiments.

Polymer substrate preparation

PDMS solutions were prepared using a Sylgard 184 silicone elastomer kit (Dow Corning) with a 10:1 ratio of base to curing agent. After mixing, the solution was degassed for 1 h until no bubbles remained. Microscope slides (Fisherbrand Adhesion Slides, Thermo Fisher, USA) were cleaned with DI water, acetone, and isopropanol. Films were cast by spin coating (Specialty Coating Systems, Inc) onto the glass slides at 1200 rpm for 25 s. The substrates were then cured in an oven at 65 °C overnight. A subset of the polymer films were soaked in either DI water (Milli-Q) or 5% wt/wt NaCl solution for 30 d. After removing the slides from the baths, the PDMS surface was rinsed with DI water and air dried for 20 min. The PDMS films for SFG experiments were spin coated at 4000 rpm for 3 min on the surface of IR grade silica prisms using the same 10:1 ratio of base to curing agent, but at lower concentration (5 % w/w PDMS in chloroform) to obtain a thickness of 370 ± 20 nm as measured by Raman spectroscopy.[30]

PDMS surface characterization

Polymer film thickness and RMS roughness values were characterized by profilometry (Bruker Dektak XT). Contact angles were measured using a goiniometer (Holmarc HO-IAD-CAM-01B). ATR-IR spectra were obtained using an FTIR (Bruker Vertex 70) fitted with a single-bounce di-

amond internal reflecting element (Pike GladiATR). Vibrational sum-frequency generation (SFG) measurements were performed using a picosecond laser (Ekspla PL2241), scanning from 2820–3020 cm^{-1} using a parametric generator (Ekspla PG501) with an s-polarized visible beam (100 μJ per pulse, bandwidth < 1 cm^{-1}) and p-polarized IR beam (300 μJ per pulse, 5 cm^{-1} bandwidth), and selecting the s-polarized component of the resulting SFG beam. We have recently demonstrated that, by precisely controlling the film thickness and beam angles in an internal reflection geometry SFG experiment, one can selectively probe either the PDMS–glass substrate or PDMS–environment (in this case, solution) interface.[30] Incident angles of $\theta_{vis} = 68^{\circ}$ and $\theta_{IR} = 78^{\circ}$ were chosen for this purpose. All of the above measurements were performed on freshly-prepared PDMS films, and those exposed to 30 d of soaking in water and 5% NaCl solution.

Flow cells

Due to the large difference in adhesion force between *B. braunii T. rotula*, two different types of flow cells were employed for our studies. For high shear rates (greater than 1000 s^{-1}), microfluidic chips were used. The chip design, shown in Figure 1a, has a channel height of 42 ± 1 μm and channel width of 5.8 mm. A pillar network was designed to break cell clusters for single cell attachment in the middle of the chip. The inlet and outlet ports were created using a 1 mm biopsy punch. The flow cell was assembled by plasma bonding (Diener Zepto One) the microfluidic top with the PDMS glass slides described above at a power of 97 W for 37 s. The devices were put in an oven immediately after bonding at 65 °C for at least 24 h prior to use. Low shear rates (less than 20 s^{-1}) were achieved using a flow cell with an 800 μm channel depth (Figure 1b) as described previously.[25]

Adhesion experiments

Regardless of whether the large height or microfluidic flow chamber was used, the basic components for the experiment are the same (Figure 1c). A syringe pump (NE-1000, New Era, USA) delivered concentrated algal culture through a 60 mL syringe for 10–15 s. This ensured there were

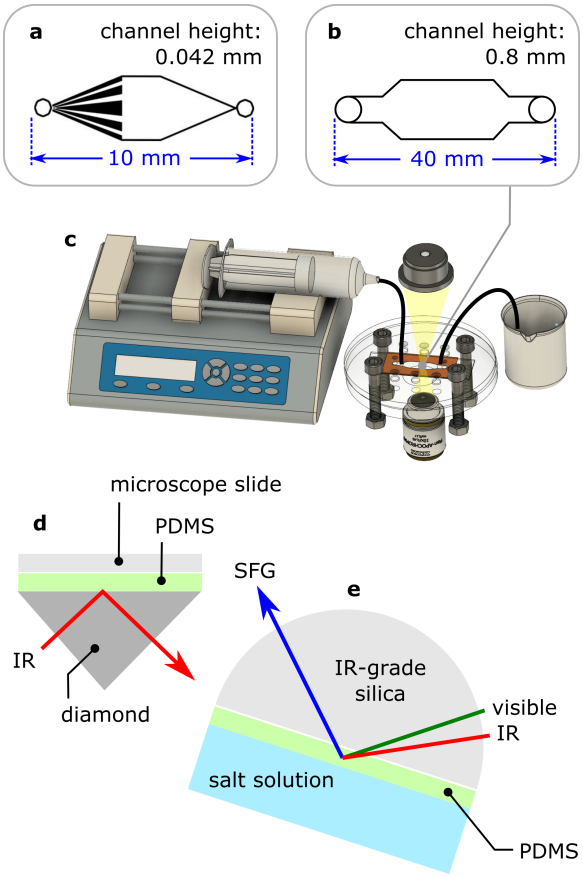

Figure 1: A laser-cut acrylic enclosure was used to secure either a (a) microfluidic or (b) large channel flow cell onto the stage of an inverted microscope to record video. (c) A computer controlled syringe pump was used to adjust the flow rate through the chamber with adhered cells. (d) ATR-IR spectroscopy and (e) visible-infrared sum-frequency generation spectroscopy were used to study the surface characteristics of the PDMS substrate following treatment.

enough cells attached to the surface that could can be incubated over the same amount of time. A 1.4 mm $\times$ 1.1 mm region in the center of the flow cell was imaged with an inverted microscope (Nikon Diphot-TMD, Nikon, USA) equipped with a 40X magnification digital camera (Amscope MD300) and a 4X objective (Nikon Fluor 4X, Nikon, USA) for in situ enumeration of attached cells. Cells that remained attached after 2 min of washout with very low flow rate (30 μL·s^{-1} for *B. braunii* and 5 μL·min^{-1} for *T. rotula*) were considered to be adhered. Cells were then allowed to rest on the surface during a 15 min incubation time, followed by gentle flushout of unadhered cells. The flow rate was then increased in a stepwise manner at pre-determined increments. When using the large flow chamber, the pump was drawing solution from the algae suspension through the flow

cell and into the syringe. In the case of the microfluidic chip, the pump direction was reversed, so the culture was preloaded into the syringe. The initial and final flow rates, Reynolds numbers (Re), and wall shear rates for each setup are listed in Table 1. We have previously described the experimental setup, including details of the video data acquisition, and image analysis including cell tracking.[25]

Table 1: Flow parameters

	Microfluidic flow chamber	Large channel flow chamber
Initial flow rate	200 μL·min^{-1}	20 μL·min^{-1}
Final flow rate	600 μL·min^{-1}	560 μL·min^{-1}
Washout flow rate	30 μL·min^{-1}	1 μL·min^{-1}
Increment	200 μL·min^{-1}	20 μL·min^{-1}
Initial Re	0.64	0.043
Final Re	4.48	1.21
Initial shear rate	1910 s^{-1}	0.44 s^{-1}
Final shear rate	13400 s^{-1}	12.44 s^{-1}

Results and Discussion

Adhesion force determination

The hydrodynamic force generated by the flow on the algal cell depends on the velocity gradient near the wall and the cell morphology.[31] Microscope images were used to measure the major and minor diameter of the cells.[32] For *B. braunii* the equivalent radius was then determined such that the equivalent sphere had the same volume as the ellipsoidal cell with the measured major and minor diameters. The circularity (C) of the cells was determined by

$$C = \frac{4\pi A}{P^2} \tag{1}$$

where A is the imaged area and P is the length of the cell perimeter. This resulted in $C = 0.82$, close to $C = 1$ for a perfect sphere, with an equivalent sphere radius of $r = 10.3 \pm 0.9$ μm. The

volumetric flow rate Q is known from the syringe pump parameters, and can be used to determine the linear flow rate

$$U = 6\frac{Q}{2hw}\frac{H}{2h}\left(1-\frac{H}{2h}\right) \tag{2}$$

where w is the channel width, h is the half-depth of the channel (see Figure 1), and H is the distance between the surface and centre of the equivalent sphere. This can then be used to determine the drag force

$$F = 6\pi f_{\mathrm{G}}\mu r U \tag{3}$$

where μ is the viscosity and $f_{\mathrm{G}} \approx 1.7$ is the Goldman wall correction factor.[33,34] Figure 2a presents the fraction of *B. braunii* that remained attached to the PDMS substrates at three different drag forces spanning approximately 5–15 nN for the three different surface preparations—no treatment (freshly prepared PDMS), and soaked in water or saline for 30 d. Under the application of the lowest drag force, most of the cells remained on the surface for the pristine and water-soaked PDMS films (p-value of 0.85). However, the films exposed to salt water for 30 d had the cell count reduced to about 15% of the initial value at 4 nN ($p < 0.05$). Under the intermediate drag force (9 nN) regime, the fraction of adhered cells for the water-soaked substrate also dropped substantially, while the pristine PDMS displayed only a minor decrease to 85% of the initial value. At the highest drag force (13 nN) the fraction of cells remaining was constant for the two soaking cases, but now the pristine PDMS also displayed a comparably low fraction of cells ($p = 0.24$ for pristine and water-soaked, $p = 0.16$ for pristine and salt-soaked).

T. rotula has coin-shaped morphology, and so a spherical approximation using Eq. 1 is not appropriate. Instead, it was modelled as a disk with a radius of $r = 12 \pm 4$ μm. There are several models that may be applied to evaluate the drag force experienced by an arbitrary-shaped object in a flow adjacent to a surface. We follow the the treatment by Brenner[25,35] to arrive at

$$F = 16 f_{\mathrm{B}}\mu r U \tag{4}$$

with the constant $f_B \approx 1.9$. Applying this expression to the linear flow rate from Eq. 2 enables the drag force on *T. rotula* to be determined. The fraction of cells remaining on the surface upon increasing drag force is shown in Figure 2b. As this is a pelagic species, we expect significantly weaker adhesion, below the level of those that can be applied with a microfluidic device, reflected in the nearly four orders of magnitude lower drag forces experienced by the cells. This regime is suitable for the application of the larger flow cell (Figure 1c). As in the case of *B. braunii*, the lowest drag force (0.4 pN) resulted in most of the cells remaining adhered for the pristine and water-soaked films; there was a reduction to 75% for the salt-soaked PDMS. however the large standard deviation in this data resulted in $p = 0.3$ in comparison to the pristine surface. At intermediate drag force (1.6 pN) both soaking conditions resulted in a substantial decrease to approximately 20% of the initial value, while adhesion on the pristine PDMS remained at 65%. A further reduction occurred upon application of the highest shear corresponding to a drag force of 2.5 pN.

Surface properties of the PDMS substrates before and after liquid exposure

It is established that the strength of cell adhesion is sensitive to the hydrophobicity of the surface.[36,37] Hydrophobic recovery of PDMS has been purported to be altered by water exposure.[38] Water contact angle and surface roughness measurements were performed to assess the hydrophobicity of the PDMS surfaces before and after DI water and salt solution exposure. The results presented in Table 2 indicate there is no significant difference between pristine PDMS surface and PDMS surfaces exposed to the liquids for 30 d, with all of the static contact angles near to 108°, in agreement with literature values.[39,40] The RMS roughness values obtained from profilometry measurements listed in Table 2 also do not reveal any differences, as they are constant in the vicinity of 20 nm. Previous studies have demonstrated an increase in roughness of silicone rubber surfaces exposed to 3% NaCl solution, but only at elevated (80 °C) temperature.[41] Finally we consider the possibility that, although PDMS is hydrophobic and does not swell appreciably, water may be trapped in the surface region after long term exposure, particularly in high ionic strength solution.[42]

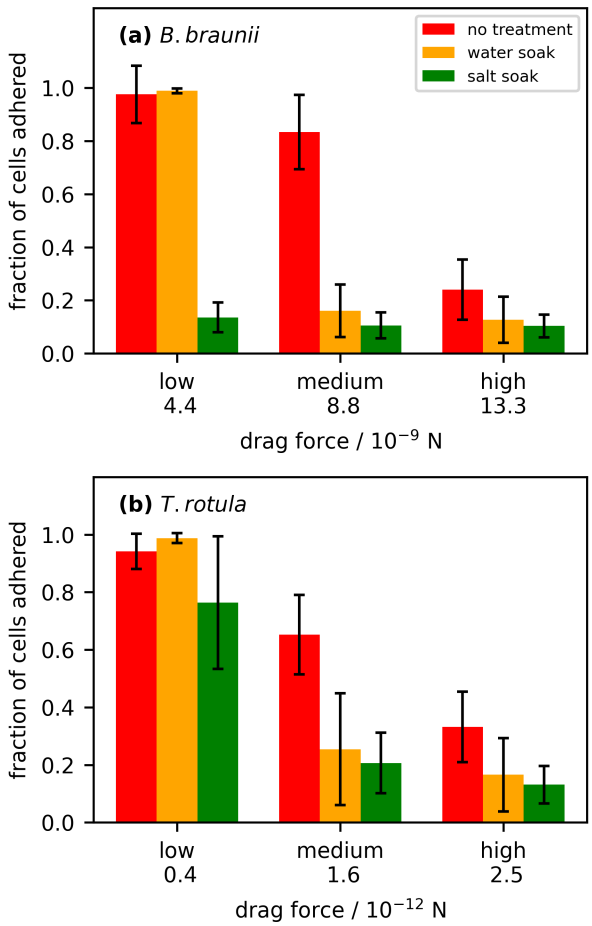

Figure 2: Fraction of cells adhered to the PDMS as a function of the drag force experienced by the cells for the three different substrate treatment conditions for (a) *B. braunii* and (b) *T. rotula*. Error bars indicate the standard deviation about the mean of three experimental replicates.

Furthermore, ATR-IR measurements have revealed differences in silicone rubber insulator surfaces exposed to salt fog and electrical stress.[43] Other studies have demonstrated that a small amount of water is incorporated in silicone elastomers, either relatively rapidly at elevated temperatures[37] or more slowly at room temperature.[44] In order to investigate whether the top layer of PDMS had some water as a result of long-term exposure, the films were placed face down onto the surface of a diamond ATR crystal and reflection absorbance spectra were recorded. In the water OH-stretching region centered around $\omega_{\mathrm{IR}} = 3400\ \mathrm{cm}^{-1}$ the refractive index of PDMS is $n_2 = 1.39 + 0.00013i$,[45] i.e. it is essentially transparent. From this, and considering a 45° angle of incidence and the

diamond refractive index n_1,[46] the evanescent wave penetration depth d_p may be calculated from

$$d_p = \frac{1}{2\pi\omega_{\mathrm{IR}}\sqrt{\sin^2\theta - (n_2/n_1)^2}} \tag{5}$$

resulting in $d_p = 0.53\ \mu$m. The absence of any water signal in the 3100–3500 cm^{-1} region, regardless of the surface exposure (Figure 3) indicates that no trapped water in the first few hundred nanometers could account for the variability in the cell adhesion forces observed.

Table 2: Contact angle and surface roughness values before and after liquid exposure.

PDMS	Contact angle	RMS roughness
no treatment	$106 \pm 6^\circ$	22 ± 13 nm
water soak	$108 \pm 2^\circ$	20 ± 7 nm
salt soak	$110 \pm 3^\circ$	20 ± 5 nm

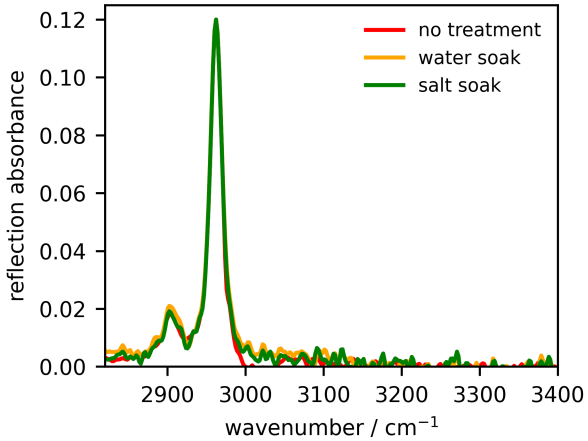

Figure 3: ATR-IR reflection absorbance spectra of the PDMS substrates with the three different treatment conditions, illustrating that there are no changes in the C–H stretching region of interest, and no signs of trapped water within the evanescent wave penetration depth.

In order to further explore whether any changes in the surface structure have occurred as a result of long-term water and salt solution exposure, we characterize the PDMS films using visible-infrared sum-frequency generation (SFG) spectroscopy. The benefit of this method is that the probing depth is governed by symmetry considerations, as opposed to the penetration depth of the beams. The bulk of the PDMS film is isotropic on account of the sample preparation conditions,

but the uppermost moieties in contact with the solution and the lowermost region in contact with the glass substrate are in unique chemical environments. This break in inversion symmetry is what generates the SFG signal. Furthermore, the selection of the film thickness and angles of incidence restrict our probe region to the film–solution interface.[30] A set of PDMS films was spin coated onto the surfaces of dove prisms and then subjected to the same soaking conditions (DI water, and 0.9 M NaCl) as the films prepared on microscope slides. As we are now able to measure directly at the buried polymer–aqueous interface, the measurement ionic strength was set to that of the growth media used in the adhesion experiments (23 mM for *B. braunii* and 250 mM for *T. rotula*). The resulting SFG spectra are shown in Figure 4. As a result of the heterogeneity often seen in the molecular orientation of polymer surfaces, the sample was translated vertically in order to collect spectra at three different spots on the polymer films. The points in Figure 4 represent the average of those three measurements, and the error bars indicate the standard deviation. Regardless of whether measurements were performed under the *B. braunii* (Figure 4a) or *T. rotula* ionic strength (Figure 4b), the PDMS methyl surface structure was fairly similar for the freshly prepared films (red) and those soaked in DI water for 30 d (orange) on account of the relative intensity of the methyl symmetric ($\omega_1 = 2909$ cm^{-1}) and antisymmetic ($\omega_2 = 2958$ cm^{-1}) modes. However, the spectra were substantially altered after 30 d of soaking in 0.9 M NaCl (green).

A more detailed analysis results from fitting the SFG spectra in order to extract the amplitude of the two methyl modes. In our experimental geometry, the recorded SFG intensity I_{SFG} encodes a single element of the effective nonlinear susceptibility $\chi^{(2)}_{\mathrm{eff}}$ through the expression

$$\begin{aligned} I_{\mathrm{SFG}} &= |\chi^{(2)}_{yyz,\mathrm{eff}}|^2 \\ &= |L_{yy}L_{yy}L_{zz}|^2 |\chi^{(2)}_{yyz}|^2. \end{aligned} \tag{6}$$

The film thickness and angles of incidence have been selected such that the local field factors L_{ii} are selective for the PDMS-solution interface.[30] After correcting for these factors, we can analyze the spectra by fixing the widths at $\Gamma_1 = 15$ cm^{-1} and $\Gamma_2 = 10$ cm^{-1}. The tilt- and twist-dependence

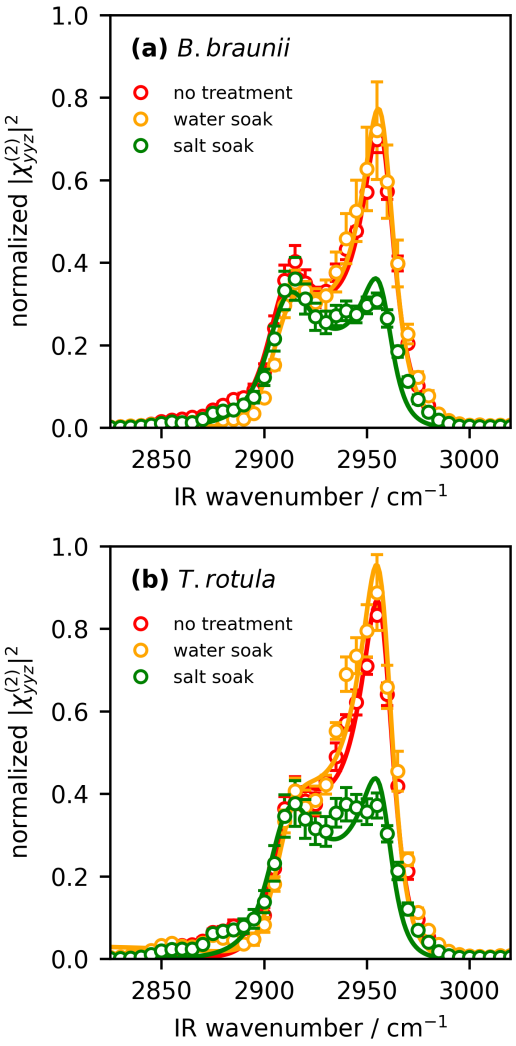

Figure 4: Visible-infrared sum-frequency spectra of the PDMS surfaces under the three treatment conditions, measured when directly exposed to NaCl with the (a) *B. braunii* and (b) *T. rotula* ionic strength from the adhesion force experiments.

of the single element $|\chi^{(2)}_{yyz}(\theta,\psi)|^2$ may then be modelled as

$$|\chi^{(2)}_{yyz}(\theta,\psi)|^2 = \left| A_{\mathrm{NR}} + \sum_{j}^{1,2} \frac{A_j(\theta,\psi)}{\omega_j - \omega_{\mathrm{IR}} - i\Gamma_j} \right|^2 \tag{7}$$

where A_{NR} is a small non-vibrationally resonant component. The resulting fit returned the amplitudes A_1 and A_2, with the modeled spectra indicated by the lines in Figure 4. If we assume that the orientation distribution is uniformly distributed about the surface normal ($C_{\infty v}$ symmetry) and the

tilt angle θ and twist angle ψ have a narrow distribution, then an orientation analysis maybe carried out based on a molecular response theory originally proposed for an isopropyl group,[47] but since extended and re-parameterized for PDMS surfaces.[18] Using the tilt and twist angle dependence of the molecular response functions developed in those accounts, we plot $A_1(\theta, \psi)$ in Figure 5a, and $A_2(\theta, \psi)$ in Figure 5b, both with filled grey contours. Overlayed onto both plots are the mathematical solutions that satisfy the experimental A_2/A_1 ratio with the red, orange and green contours corresponding to the PDMS surface treatment. Here the solid lines indicate the *B. braunii* values, and the dashed contours indicate the *T. rotula* values. It is evident that a continuous large range of (θ, ψ) are consistent with the experimental data, so we seek to implement additional constraints: we search for the solutions along the red (no soaking treatment) contour that move to any locations on the water soak (orange) or salt soak (green) contours that are also consistent with the relative amplitude change for A_1 and A_2 when the surface treatment changes. These (θ, ψ) values are indicated with points in Figure 5. The relative orientation and position of the two methyl groups connected to the Si atom are shown in Figure 6. One first notices that, upon increasing the *measurement* ionic strength (comparing the two sets of solutions circled in Figure 5a) the twist angle is relatively constant, but the plane of the methyl groups reorients to a larger tilt angle. Within a single measurement ionic strength (either algae species), water soaking causes the twist angle to increase with only minor changes in tilt angle, while 0.9 M salt soaking causes the twist angle to decrease while again the tilt angle is mostly unaffected. The differences in the appearance of the spectra in Figure 4 are therefore due to the consequence of such a twist angle change according to the PDMS treatment condition.

Perspective

It has been suggested that the reorientation of PDMS surface groups may be responsible for loss of hydrophobicity when exposed to solution environments.[44] For either alga under the corresponding measurement ionic strength (according to the appropriate environmental/growth medium), cells on the pristine PDMS surface are exposed to methyl groups that are twisted in an orientation that

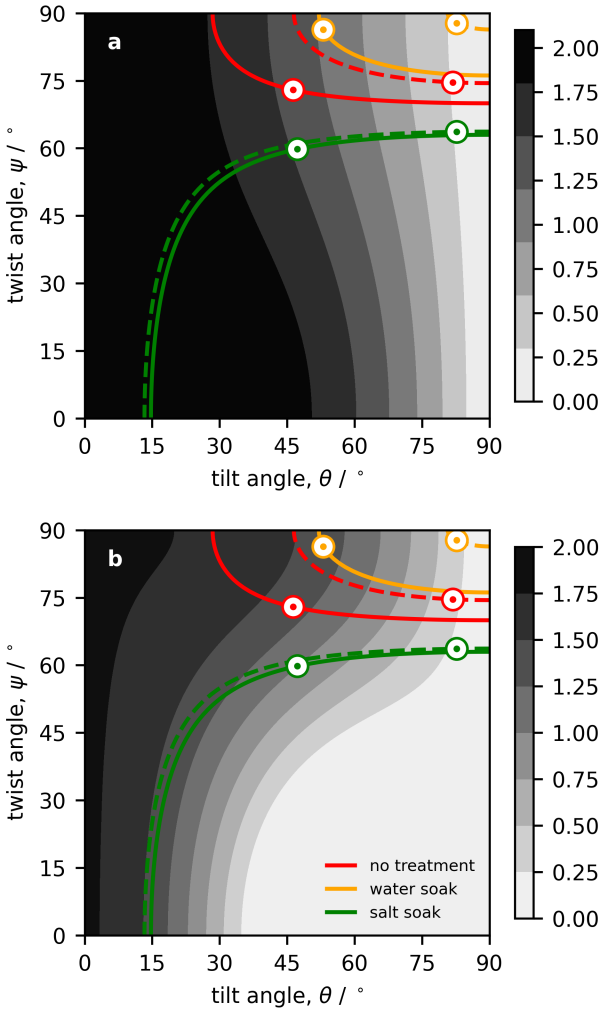

Figure 5: (a) PDMS methyl symmetric stretch amplitude A_1 and (b) negative regions antisymmetric stretch amplitude A_2 as a function of the joint tilt and twist angle, plotted with filled grey contours. The set of solutions that satisfy the amplitude ratio A_2/A_1 is overlayed with coloured contours, where the solid lines correspond to the *B. braunii* ionic strength, and dashed lines to the *T. rotula* ionic strength. Solutions that are consistent with both the ratios and and the amplitude trends for both peaks are indicated with points. The width of the white circles around the points indicates the uncertainty based on the constrained search algorithm.

places them at different distances with respect to the solid–liquid interface (Figure 6a). After soaking in water for 30 d the methyl groups, when probed in an aqueous salt solution, reorient so they are closer to equidistant to the surface plane (Figure 6b). Salt soaking increases the twist of the plane, so that one methyl group is now directed more towards the bulk PDMS phase, while another methyl group is more oriented towards the aqueous phase (Figure 6c). Our observations

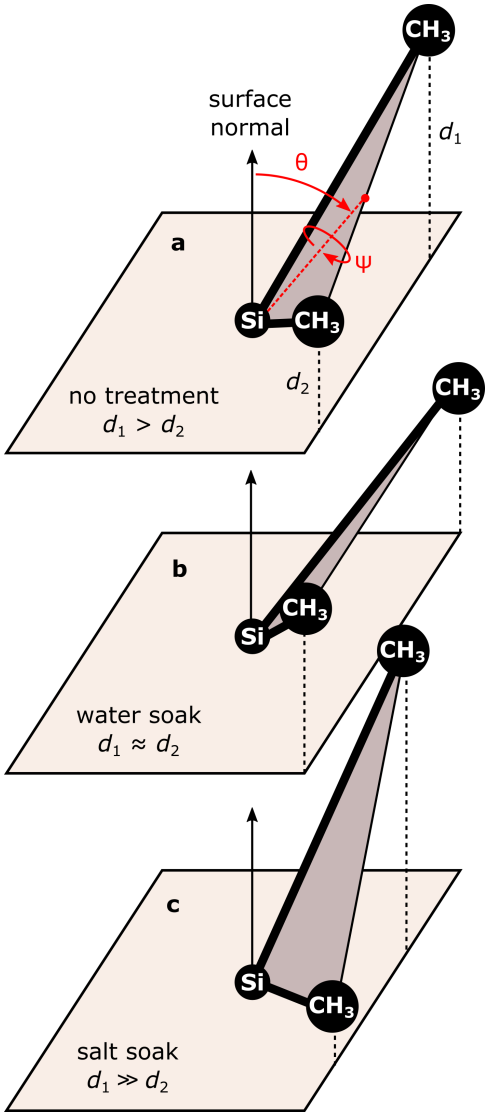

Figure 6: Tilt (θ) and twist (ψ) angles of the plane defined by the two methyl C_3 axes. The twist is about the vector from the origin (Si atom) to midpoint (red dot) between the two carbon atoms. The tilt angle has been determined to be a function of the measurement ionic strength only, while the twist angle is altered by the PDMS aqueous exposure. (a) Initially the plane is twisted so the two methyl groups are at different distances with respect to the surface. (b) Water exposure increases the twist angle so the methyl groups are closer to equidistant to the surface. (c) Saline exposure reduces the twist angle so that the environment between the two methyl groups becomes more dissimilar.

suggest that the change in twist angle from $\psi = 70^\circ$ to $\psi = 85^\circ$ after water soaking does not have an appreciable effect on algae adhesion to PDMS. It is reasonable that both of these orientations have the methyl groups roughly equidistant to the plane of the surface. However, the change to $\psi = 60^\circ$ upon salt soaking might affect the cell-surface interactions in a manner that is analogous

to a decrease in hydrophobilcity, but not to an extent that is revealed by the contact angle. Previous studies have determined that hydrophobic recovery is inhibited in water compared to the PDMS–air interface, and that the extent to which hydrophobic groups reorient and diffuse to the surface is even more limited for PDMS next to sea water.[38] We further speculate that this may have a more pronounced influence for *B. braunii* as it has a higher affinity for PDMS. The mechanism behind this water- and salt-induced reorientation of PDMS surface methyl groups is not clear. However, molecular dynamics studies have shown that penetration of chloride ions into the polymer is significantly greater than either sodium ions or water molecules, and could trigger changes in the polymer structure.[48]

At intermediate drag forces, soaking the PDMS in either water or salt solution resulted in a reduction of adhered cells compared to the pristine PDMS substrates. This result is difficult to explain using our data. As our shear values were all below 1.5×10^4 s^{-1}, we have been assuming that the cells are in contact with similar surface conditions while they experience varying drag forces. The effect of liquid flow on interfacial structure has been explored,[49–53] but no such study has been performed for PDMS. Kurian et al. have observed an increase in the PDMS surface methyl orientation when friction was applied to the polymer surface directly by mechanical contact.[22] Further work to probe the effect of liquid-induced shear at the PDMS surface may be necessary to provide a microscopic description of the PDMS surface under such intermediate shear. At the highest shear rates and highest drag forces experienced by the cells, the differences in PDMS surface treatment were much smaller, indicating that the molecular-level surface details such as methyl group orientation are not as relevant to the algae adhesion.

We now consider the implications of these findings to electrical power insulators that benefit from reduced adhesion of algae in order to prolong their hydrophobicity. Our findings have revealed that, for the freshwater alga *B. braunii*, long-term exposure to salt (such as in winter conditions near roads where deicing agents are used) reduces algae adhesion, especially at low drag forces. The low shear regime is the one encountered in typical environmental conditions. For example, wind and rain shear is less than 0.01 s^{-1}.[54–56] These results show that there is no

substantial difference in adhesion resistance for water exposure, for example due to rain alone. Near ocean coastal areas, high salinity environments result from sea water spray onto insulator surfaces. For the seawater species *T. rotula*, PDMS exposure to high salt concentration shows only minor reduction in algae adhesion in the ultra-low shear regime, and both water and salt exposure have less drastic consequences at higher shear rates. Accounting for these differences requires an understanding of the polymer surface conditions when directly exposed to the environment in which the cells are present.

Conclusions

Silicone-based polymers are being evaluated as candidates for next-generation insulators for overhead power distribution, replacing glass and ceramic materials particularly in environments where water and salt exposure are common. This work has illustrated that liquid conditions can affect the PDMS surface structure, and this in turn has consequences on cell adhesion. Surface chemical group orientation is known to play an important role in the chemical and physical properties of surfaces. However, such changes often do not show up in macroscopic probes such as contact angle or surface roughness measurements. The combination of lateral flow drag force experiments and surface characterization using a combination of macroscopic and molecular-level nonlinear optical probes have revealed subtle differences in polymer surface structure that are relevant to adhered cells.

Acknowledgement

This project was supported by the Natural Sciences and Engineering Research Council of Canada (NSERC) through Discovery, Collaborative Research and Discovery (CRD), and Alliance grants to DKH, in partnership with ASAsoft Canada Inc. *B. braunii* cultures were maintained at the Centre of Advanced Materials and Related Technologies (CAMTEC) at the University of Victoria, with assistance from the CAMTEC Facility for Biological Sample Preparation manager, Rebecca

Hof. *T. rotula* parent cultures were grown and maintained in incubation chambers in the laboratory of DEV. Ben MacVicar developed the software used for the flow cell data collection and algae tracking image analysis.

References

(1) Ghosh, D.; Khastgir, D. Degradation and Stability of Polymeric High-Voltage Insulators and Prediction of Their Service Life through Environmental and Accelerated Aging Processes. *ACS Omega* **2018**, *3*, 11317–11330.

(2) Ghosh, D.; Bhandari, S.; Chaki, T. K.; Khastgir, D. Development of a High Performance High Voltage Insulator for Power Transmission Lines from Blends of Polydimethylsiloxane/ethylene Vinyl Acetate Containing Nanosilica. *RSC Adv.* **2015**, *5*, 57608–57618.

(3) Hillborg, H.; Gedde, U. W. Hydrophobicity Changes in Silicone Rubbers. *IEEE Trans. Dieletr. Electr. Insul.* **1999**, *6*, 703–717.

(4) Bengtsson, M.; Grönlund, R.; Lundqvist, M.; Larsson, A.; Kröll, S.; Svanberg, S. Remote Laser-Induced Breakdown Spectroscopy for the Detection and Removal of Salt on Metal and Polymeric Surfaces. *Appl. Spectrosc.* **2006**, *60*, 1188–1191.

(5) Farzaneh, M.; Baker, A. C.; Bernstorf, R. A.; Burnhan, J. T.; Cherney, E. A.; Chisholm, W. A.; Fofana, I.; Gorur, R. S.; Grisham, T.; Gutman, I.; Rolfseng, L.; Stewart, G. A. Selection of Line Insulators with Respect to Ice and Snow—Part I: Context and Stresses. *IEEE Trans. Power Delivery* **2007**, *22*, 2289–2296.

(6) Wallströma, S.; Dowling, K.; Karlsson, S. Development and Comparison of Test Methods for Evaluating Formation of Biofilms on Silicones. *Polym.* **2002**, *78*, 257–262.

(7) Wallström, S.; Karlsson, S. Biofilms on Silicone Rubber Insulators; Microbial Composition and Diagnostics of Removal by Use of ESEM/EDS: Composition of Biofilms Infecting Silicone Rubber Insulators. *Polym. Degrad. Stabil.* **2004**, *85*, 841–846.

(8) Xie, C.; Li, C.; Zhu, W.; Gan, Y. Analysis of Green Algae Contamination on 500kV Silicone Rubber Composite Insulators. *Int. Conf. Electrical Materials and Power Equipment* **2017**, *1*, 664–666.

(9) Ouyang, X.; Yin, F.; Jia, Z.; Yang, S.; Wang, Y.; Bai, H.; Zhang, X.; Li, Y.; Chen, H. Research of Biological Contamination and its Effect on the Properties of RTV-Coated Insulators. *Electr. Pow. Syst. Res.* **2019**, *167*, 138–149.

(10) Yang, S.; Jia, Z.; Ouyang, X.; Wang, S. Inhibition of Algae Growth on HVDC Polymeric Insulators using Antibiotic-Loaded Silica Aerogel Nanocomposites. *Poly. Degrad. Stab.* **2018**, *155*, 262–270.

(11) Yang, S.; Jia, Z.; Ouyanga, X.; Bai, H.; Liu, R. Hydrophobicity Characteristics of Algae-Fouled HVDC Insulators in Subtropical Climates. *Electr. Power Syst. Res.* **2018**, *163*, 626–637.

(12) Kim, H. S.; Weiss, T. L.; Thapa, H. R.; Devarenne, T. P.; Han, A. A Microfluidic Photobioreactor Array Demonstrating High-Throughput Screening for Microalgal Oil Production. *Lab Chip* **2014**, *14*, 1415–1425.

(13) Siddiquie, R. Y.; Gaddam, A.; Agrawal, A.; Dimov, S. S.; Joshi, S. S. Anti-Biofouling Properties of Femtosecond Laser-Induced Submicron Topographies on Elastomeric Surfaces. *Langmuir* **2020**, *36*, 5349–5358.

(14) Chen, Z.; Shen, Y. R.; Somorjai, G. A. Studies of Polymer Surfaces by Sum Frequency Generation Vibrational Spectroscopy. *Annu. Rev. Phys. Chem.* **2002**, *53*, 437–465.

(15) Zuo, B.; Hu, Y.; Lu, X.; Zhang, S.; Fan, H.; Wang, X. Surface Properties of Poly(vinyl alcohol) Films Dominated by Spontaneous Adsorption of Ethanol and Governed by Hydrogen Bonding. *J. Phys. Chem. C* **2013**, *117*, 3396–3406.

(16) Zhang, W.; Zhang, Z.; Wang, X. Investigation on Surface Molecular Conformations and Pervaporation Performance of the Poly(vinyl alcohol) (PVA) Membrane. *J. Coll. Interf. Sci.* **2009**, *333*, 346–353.

(17) Defante, A. P.; Burai, T. N.; Becker, M. L.; Dhinojwala, A. Consequences of Water between Two Hydrophobic Surfaces on Adhesion and Wetting. *Langmuir* **2015**, *31*, 2398–2406.

(18) Zhang, C.; Chen, Z. Probing Molecular Structures of Poly(Dimethylsiloxane) at Buried Interfaces In Situ. *J. Phys. Chem. C* **2013**, *117*, 3903–3914.

(19) Ye, H.; Gu, Z.; Gracias, D. Kinetics of Ultraviolet and Plasma Surface Modification of Poly(dimethylsiloxane) Probed by Sum Frequency Vibrational Spectroscopy. *Langmuir* **2006**, *22*, 1863–1868.

(20) Chen, C.; Wang, J.; Chen, Z. Surface Restructuring Behavior of Various Types of Poly(dimethylsiloxane) in Water Detected by SFG. *Langmuir* **2004**, *20*, 10186–10193.

(21) Shi, Q.; Ye, S.; Spanninga, S. A.; Su, Y.; Jiang, Z.; Chen, Z. The Molecular Surface Conformation of Surface-tethered Polyelectrolytes on PDMS Surfaces. *Soft Matter* **2009**, *18*, 3487–3494.

(22) Kurian, A.; Prasad, S.; Dhinojwala, A. Unusual Surface Aging of Poly(dimethylsiloxane) Elastomers. *Macromolecules* **2010**, *43*, 2438–2443.

(23) Kaur, H.; Tomar, D.; Kaur, H.; Rana, B.; Chaudhary, S.; Jena, K. C. Sum-Frequency Generation Vibrational Spectroscopy: A Nonlinear Optical Tool to Probe the Polymer Interfaces. Advances in Spectroscopy: Molecules to Materials. Singapore, 2019; pp 39–55.

(24) Strazdaite, S.; Versluis, J.; Backus, E. H. G.; Bakker, H. J. Enhanced ordering of water at hydrophobic surfaces. *J. Chem. Phys.* **2014**, *140*, 054711.

(25) Wan, Z.; MacVicar, B. T.; Wyatt, S.; Varela, D. E.; Padmawar, R.; Hore, D. K. An Automated Image Analysis Platform for the Study of Weakly-Adhered Cells. *Biofouling* **2021**, *37*, 387–396.

(26) Hasle, G. R. The Biogeography of Some Marine Planktonic Diatoms. *Deep Sea Res. Oceanogr. Abstr.* **1976**, *23*, 319–338.

(27) Leblanc, K. et al. A Global Diatom Database—Abundance, Biovolume and Biomass in the World Ocean. *Earth Syst. Sci. Data* **2012**, *4*, 149–165.

(28) Andersen, R. A. *Algal Culturing Techniques*; Elsevier: Burlington, 2005.

(29) Berges, J.; Franklin, D.; Harrison, P. Evolution of an Artificial Seawater Medium: Improvements in Enriched Seawater, Artificial Water Over the Last Two Decades. *J. Phycology* **2001**, *37*, 1138–1145.

(30) Azam, M. S.; Cai, C.; Hore, D. K. Selective Probing of Thin-Film Interfaces Using Internal Reflection Sum-Frequency Spectroscopy. *J. Phys. Chem. C* **2019**, *123*, 23535–23544.

(31) Busscher, H. J.; van der Mei, H. C. Microbial Adhesion in Flow Displacement Systems. *Clin. Microbiol. Rev.* **2006**, *19*, 127–141.

(32) Schneider, C. A.; Rasband, W. S.; Eliceiri, K. W. NIH Image to ImageJ: 25 Years of Image Analysis. *Nat. Methods* **2012**, *9*, 671–675.

(33) Wiklund, K.; Zhang, H.; Stangner, T.; Singh, B.; Bullitt, E.; Andersson, M. A Drag Force Interpolation Model for Capsule-Shaped Cells in Fluid Flows Near a Surface. *Microbiol.* **2018**, *164*, 483–494.

(34) Bos, R.; C., H.; van der Mei,; Busscher, H. J. Physico-Chemistry of Initial Microbial Adhesive Interactions–Its Mechanisms and Methods for Study. *FEMS Microbiol. Rev.* **1999**, *23*, 179–230.

(35) Brenner, H. Effect of Finite Boundaries on the Stokes Resistance of an Arbitrary Particle. *J. Fluid Mech.* **1962**, *12*, 35–48.

(36) Song, W.; Mano, J. F. Interactions Between Cells or Proteins and Surfaces Exhibiting Extreme Wettabilities. *Soft Matter* **2013**, *9*, 2985–2999.

(37) Park, J. Y.; Ahn, D.; Choi, Y. Y.; Hwang, C. M.; Takayama, S.; Lee, S. H.; Lee, S.-H. Surface Chemistry Modification of PDMS Elastomers with Boiling Water Improves Cellular Adhesion. *Sens. Actuators B* **2012**, *173*, 765–771.

(38) Bausch, G. G.; Stasser, J. L.; Tonge, J. S.; Owen, M. J. Behavior of Plasma-Treated Elastomeric Polydimethylsiloxane Coatings in Aqueous Environment. *Plasma Polym.* **1998**, *3*, 23–34.

(39) Berdichevsky, Y.; Khandurina, J.; Guttman, A.; Lo, Y.-H. UV/Ozone Modification of Poly(dimethylsiloxane) Microfluidic Channels. *Sens. Actuators B* **2004**, *97*, 402–408.

(40) Ruben, B.; Elisa, M.; Leandro, L.; Victor, M.; Gloria, G.; Marina, S.; Mian, S.; Pandiyan, R.; Nadhira, L. Oxygen Plasma Treatments of Polymethylsiloxane Surfaces: Effect of the Atomic Oxygen on Capillary Flow in the Microchannels. *Micro Nano Lett.* **2017**, *12*, 754–757.

(41) Allen, B.; Bleszynski, M.; Kumosa, M.; Willis, E. Investigation into the Effects of Environmental Stresses on RTV-1 Silicone-based Caulk Materials. *IEEE Trans Dielectr Electr Insul* **2015**, *22*, 2978–2986.

(42) Bacchin, P.; Marty, A.; Duru, P.; Meireles, M.; Aimar, P. Colloidal Surface Interactions and Membrane Fouling: Investigations at Pore Scale. *Adv. Coll. Interf. Sci.* **2011**, *164*, 2–11.

(43) Kim, S.-H.; Cherney, E. A.; Hackam, R. Hydrophobic Behavior of Insulators Coated with RTV Silicone Rubber. *IEEE Trans. Electr. Insul.* **1992**, *27*, 610–622.

(44) Lee, S. H.; Ruckenstein, E. Surface Restructuring of Polymers. *J. Coll. Interfacial Sci.* **1987**, *120*, 529–536.

(45) Zhang, X.; Qiu, J.; Zhao, J.; Li, X.; Liu, L. Complex Refractive Indices Measurements of Polymers in Infrared Bands. *J. Quant. Spectrosc. Radiat. Transfer* **2020**, *252*, 107063.

(46) Phillip, H. R.; Taft, E. A. Kramers-Kronig Analysis of Reflectance Data for Diamond. *Phys. Rev.* **1964**, *136*, A1445–A1448.

(47) Kataoka, S.; Cremer, P. S. Probing Molecular Structure at Interfaces for Comparison with Bulk Solution Behavior: Water/2-Propanol Mixtures Monitored by Vibrational Sum Frequency Spectroscopy. *J. Am. Chem. Soc.* **2006**, *128*, 5516–5522.

(48) Bleszynski, M.; Kumosa, M. Silicone Rubber RTV-1 Aging in the Presence of Aqueous Salt. *IEEE Trans Dielectr Electr Insul* **2016**, *23*, 2822–2829.

(49) Lis, D.; Backus, E. H. G.; Hunger, J.; Parekj, S. H.; Bonn, M. Liquid flow along a solid surface reversibly alters interfacial chemistry. *Science* **2014**, *344*, 1138–1142.

(50) Schrödle, S.; Richmond, G. R. Equilibrium and Non-equilibrium kinetics of Self-Assembled surfactant Monolayers: A vibrational Sum-Frequency Study of Dodecanoate at the Fluorite–Water Interface. *J. Am. Chem. Soc.* **2008**, *130*, 5072–5085.

(51) Yu, C.; Evmenenko, G.; Kmetko, J.; Dutta, P. Effects of Shear Flow on Interfacial Ordering in Liquids: X-ray Scattering Studies. *Langmuir* **2003**, *19*, 9558–9561.

(52) Goffin, A. J. J.; Rajadas, J.; Fuller, G. G. Interfacial Flow Processing of Collagen. *Langmuir* **2010**, *26*, 3514–3521.

(53) Cheng, H.-W.; Weiss, H.; Stock, P.; Chen, Y.-J.; Reinecke, C. R.; Dienemann, J.-N.; Mezger, M.; Valtiner, M. Effect of Concentration on the Interfacial and Bulk Structure of Ionic Liquids in Aqueous Solution. *Langmuir* **2018**, *34*, 2637–2646.

(54) Lien, R.-C.; Henyey, F.; Ma, B.; Yang, Y. J. Large-Amplitude Internal Solitary Waves Observed in the Northern South China Sea: Properties and Energetics. *J. Phys. Oceanogr.* **2014**, *44*, 1095–1115.

(55) Peters, H.; Gregg, M. C.; Sanford, T. B. On the Parameterization of Equatorial Turbulence: Effect of Fine-Scale Variations Below the Range of the Diurnal Cycle. *J. Geophys. Res.* **1995**, *100*, 18333–18348.

(56) Wenegrat, J. O.; McPhaden, M. J.; Lien, R.-C. Wind Stress and Near-Surface Shear in the Equatorial Atlantic Ocean. *Geophys. Res. Lett.* **2014**, *41*, 1226–1231.

Graphical TOC Entry